Electronic Supplementary Material (ESI) for Nanoscale Advances.
This journal is © The Royal Society of Chemistry 2022

Supplementary Information: Direct observation of narrow electronic energy band formation in 2D molecular self-assembly

Jack Hellerstedt,[†,@] Marina Castelli,[†,‡,@] Anton Tadich,[¶] Antonija Grubišić - Čabo,[†] Dhaneesh Kumar,[†,‡] Benjamin Lowe,[†,‡] Spiro Gicev,[§] Dionysios Potamianos,[‖] Maximilian Schnitzenbaumer,[‖] Pascal Scigalla,[‖] Simiam Ghan,[⊥] Reinhard Kienberger,[‖] Muhammad Usman,[§,#] and Agustin Schiffrin[*,†,‡]

†*School of Physics and Astronomy, Monash University, Clayton Victoria 3800, Australia*

‡*ARC Centre of Excellence in Future Low-Energy Electronics Technologies, Monash University, Clayton Victoria 3800, Australia*

¶*Australian Synchrotron, 800 Blackburn Road, Clayton Victoria 3168, Australia*

§*Centre for Quantum Computation and Communication Technology, School of Physics, The University of Melbourne, Parkville Victoria 3010, Australia*

‖*Physik-Department, Technische Universität München, 85748 Garching, Germany*

⊥*Chair for Theoretical Chemistry and Catalysis Research Center, Technical University of Munich, Lichtenbergstraße 4, D-85747 Garching, Germany*

#*School of Computing and Information Systems, Melbourne School of Engineering, The University of Melbourne, Parkville Victoria 3010, Australia*

@*These authors contributed equally*

E-mail: agustin.schiffrin@monash.edu

Contents

S1 Ag(100) reference photoelectron spectroscopy

S1.1 ARPES Constant Binding Energy (CBE) maps

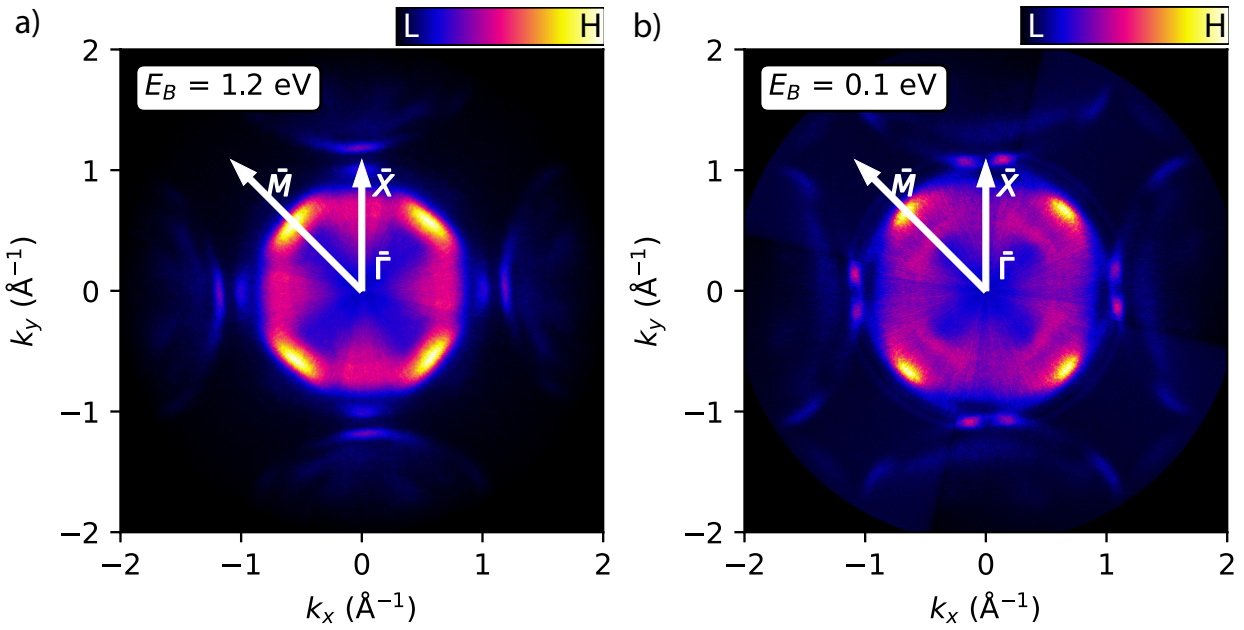

Figure S1: **Reference ARPES CBE maps of clean Ag(100).** **a:** At $E_B = 1.2$ eV (corresponding to MgPc ML and 2L HOMO; main text Fig. 3b, c). **b:** At $E_B = 0.1$ eV (corresponding to MgPc ML LUMO; main text Fig. 3a). White arrows label Ag(100) high symmetry directions.

S1.2 ARPES Energy Distribution Curves (EDCs)

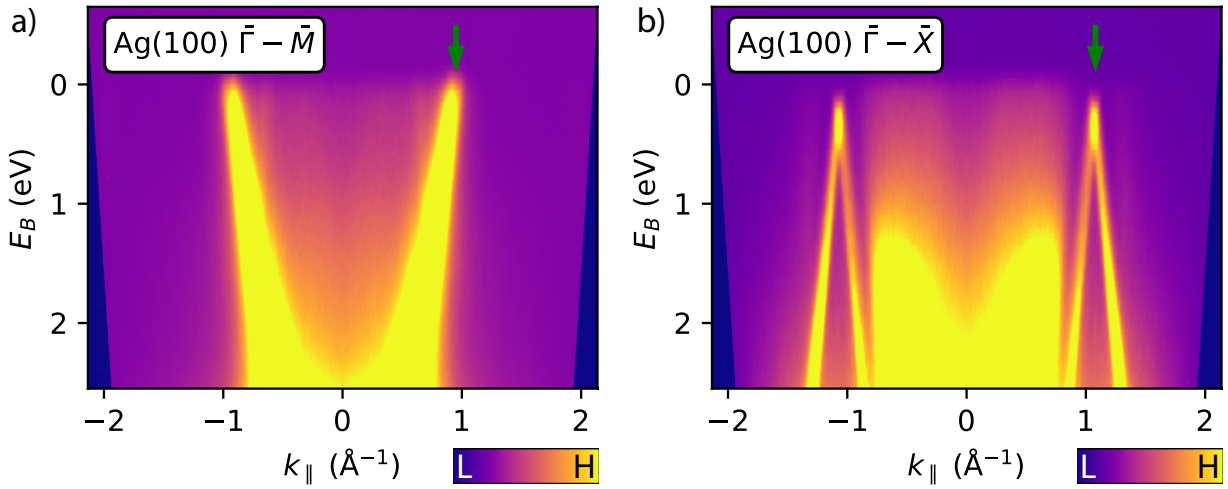

Figure S2: **Reference ARPES EDCs of clean Ag(100).** **a, b:** ARPES intensity, $I(E_\mathrm{B}, k_\parallel)$, as a function of $k_\parallel$ and E_B, for $\mathbf{k}_\parallel$ along Ag(100) $\bar{\Gamma} - \bar{M}$ (a) and $\bar{\Gamma} - \bar{X}$ (b) orientations. Green arrows: Ag *sp*-band features. Data symmetrized with respect to $k_\parallel = 0$ due to non-normal incidence of UV beam, i.e., $I(E_\mathrm{B}, k_\parallel) = I(E_\mathrm{B}, -k_\parallel)$ (see Methods in main text).

S2 MgPc Bilayer (2L): ARPES EDCs and Tight-Binding (TB) Model

Similar to the ML (Fig. 4 in main text), we acquired ARPES intensity data, $I(E_{\mathrm{B}}, k_{\parallel})$, as a function of E_{B}, for $\mathbf{k}_{\parallel}$ along the Ag(100) $\bar{\Gamma} - \bar{M}$ and $\bar{\Gamma} - \bar{X}$ orientations, for the 2L (Fig. S3a, b). We fit $I(E_{\mathrm{B}}, k_{\parallel})$ for E_{B} within the range [~ 0.6 eV, ~ 2 eV] related to the HOMO, for different $k_{\parallel}$ values, with a single Gaussian peak and a Shirley background (Fig. S3c, d). The full-width-at-half-maximum (FWHM) of this 2L HOMO Gaussian peak is 478 ± 6 meV, larger than that for the ML (401 ± 6 meV; see main text). This increase in FWHM could be explained by the photon beam spot size (>100 μm) and sampling depth including contributions from the underlying ML.

Similar to the ML (Fig. 4e, f in main text), the E_{B} position of this 2L HOMO Gaussian peak varies with $k_{\parallel}$ (Fig. S3 e, f). We fit this experimental 2L HOMO E_{B} positions for $\mathbf{k}_{\parallel}$ along the Ag(100) $\bar{\Gamma} - \bar{M}$ (Fig. S3e) and $\bar{\Gamma} - \bar{X}$ (Fig. S3f) directions with $E(k_x, k_y)$ (Eqn. 2 of the main text) resulting from the single-band (i.e., one HOMO per MgPc film unit cell) nearest-neighbor tight-binding (TB) model. This fit yields an intermolecular hopping integral $t = -5.2 \pm 0.2$ meV (compared to -2.5 meV for the ML), and, for $\mathbf{k}_{\parallel}$ along $\bar{\Gamma} - \bar{M}$, a MgPc 2L top-layer lattice constant $b = 15.2$ Å and an angle $\alpha = 32.6 \pm 2^{\circ}$ between MgPc 2L top-layer and Ag(100) unit cell vectors ($b = 16$ Å and $\alpha = 27 \pm 2^{\circ}$ along $\bar{\Gamma} - \bar{X}$). The bandwidth $BW = 8|t|$ of this HOMO-related energy dispersion for the 2L seems twice that for the ML; this could be explained by some degree of interlayer π-stacking.[1,2] The $\sim$10 meV offset of the average HOMO E_{B} position for the 2L along the Ag(100) $\bar{\Gamma} - \bar{M}$ orientation (Fig. S3e) is likely due to a change in PES signal background noise for that scan.

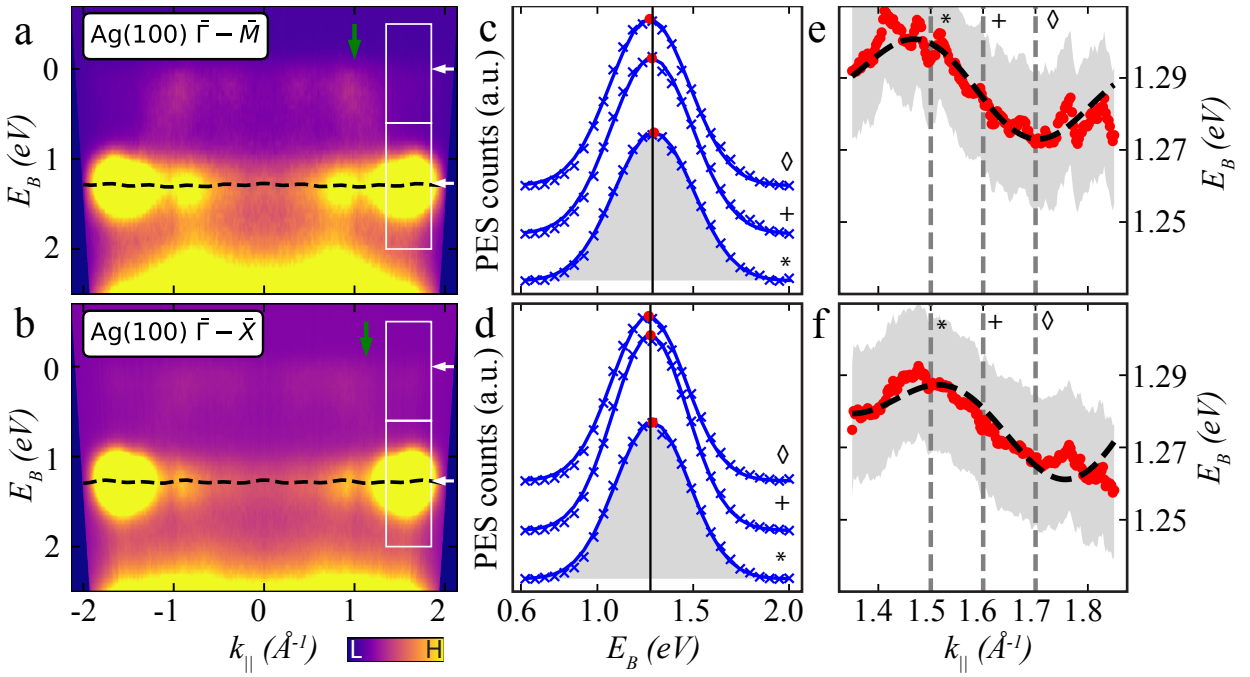

Figure S3: **ARPES energy distribution curves (EDCs) of MgPc bilayer (2L) on Ag(100).** **a, b:** ARPES intensity, $I(E_\mathrm{B}, k_{||})$, as a function of $k_{||}$ and E_B, measured for $\mathbf{k}_{||}$ along Ag(100) $\bar{\Gamma}-\bar{M}$ (a) and $\bar{\Gamma}-\bar{X}$ (b) azimuthal orientations. White boxes: $k_{||}$ and E_B ranges related to LUMOs and HOMO. Green arrows: Ag *sp*-band features. Black dashed line: tight-binding HOMO-related energy dispersion for full $k_{||}$ range [using same fitted parameters as in (e, f)]. **c, d:** ARPES intensity, $I(E_\mathrm{B}, k_{||})$, as a function of E_B for different $\mathbf{k}_{||}$ [related to HOMO; lower boxes in (a, b)] along Ag(100) $\bar{\Gamma}-\bar{M}$ (c) and $\bar{\Gamma}-\bar{X}$ (d) orientations. Curves offset for clarity. Blue crosses: experimental data after Shirley background subtraction; blue curves: single Gaussian peak fit (shaded grey area); red dots: fit Gaussian peak energy positions; black vertical line: average Gaussian peak energy position. Symbols match curves to $k_{||}$ values indicated by grey vertical dashed lines in (e, f). **e, f:** Energy positions of HOMO-related fit Gaussian peak versus $k_{||}$ along Ag(100) $\bar{\Gamma}-\bar{M}$ (e) and $\bar{\Gamma}-\bar{X}$ (f) orientations (red dots). Grey shaded regions: Gaussian peak fit standard error plus k_BT ($T = 293$ K, accounting for room temperature thermal broadening) for each data point. Dashed black curve: fit resulting from single-band tight-binding model. The ∼10 meV offset of the average HOMO E_B position for $\bar{\Gamma}-\bar{M}$ (e) relative to $\bar{\Gamma}-\bar{X}$ (f) as well as the ML (main text Fig. 4) is likely due to a change in PES signal background noise for that scan.

S3 TB Model Intermolecular Hopping Integral t: Fit vs. Calculation

We compared the TB inter-HOMO hopping integral $t = -2.5 \pm 0.2$ (ML) and -5.2 ± 0.2 meV (2L), retrieved from fitting the experimental HOMO E_{B} positions for $\mathbf{k}_{\parallel}$ along the Ag(100) $\bar{\Gamma} - \bar{M}$ and $\bar{\Gamma} - \bar{X}$ directions (main text Fig. 4e, f for ML; Fig. S3e, f for 2L) with $E(k_x, k_y)$ in main text Eqn. 2, with the value of t calculated as

$$t = \left\langle \Psi^{(j\pm1)}_{\mathrm{HOMO}} | H_{\mathrm{int}} | \Psi^{(j)}_{\mathrm{HOMO}} \right\rangle \tag{1}$$

Here, $\Psi^{(j)}_{\mathrm{HOMO}}$ and $\Psi^{(j\pm1)}_{\mathrm{HOMO}}$ are nearest-neighbour HOMOs (at sites j and $j \pm 1$ within the MgPc ML) calculated by DFT in the gas phase (inset main text Fig. 3b), and H_{int} is an effective Coulomb interaction Hamiltonian between $\Psi^{(j)}_{\mathrm{HOMO}}$ and $\Psi^{(j\pm1)}_{\mathrm{HOMO}}$. In $H_{\mathrm{int}} = -\frac{\beta e^2}{4\pi\epsilon_0} \frac{1}{|\mathbf{r} - \mathbf{r}^{(j\pm1)}_{\mathrm{Mg}}|}$ (determined in previous work[3]), $\beta \approx 5.9$ is a unitless constant that determines the strength of the inter-MgPc interaction, $\mathbf{r}^{(j\pm1)}_{\mathrm{Mg}}$ is the position vector of the nearest-neighbor MgPc centre, e is the electron charge and ϵ_0 is the vacuum permittivity. This calculation, in which we considered the structural properties of the MgPc ML (i.e., MgPc ML unit cell vectors, molecular orientation within ML) as determined by SPM and LEED measurements (main text Fig. 1), yields $t \approx 10^{-5}$ eV. The calculated value of t (for the DFT-calculated gas-phase HOMO) becomes more substantial, on the order of a few meV's ($\sim$3 meV, consistent with experiment), when the ML lattice constant is reduced by $\sim$2 Å (from $b = 15.3$ to 13 Å, i.e., by $\sim$10%), and when the angle between MgPc isoindole-isoindole axis and MgPc film unit cell vectors is slightly altered (28.5°, compared to measured 29°). Based on a previous study,[3] the fact that our experiments suggest a value of t for the ML two orders of magnitude larger than the calculated t can be explained by electronic hybridization between MgPc and underlying metal, which can lead to the spatial extension of $\Psi_{\mathrm{HOMO}}(\mathbf{r})$, resulting in an increase of inter-HOMO overlap and hence in a significantly larger observed t. That is, assuming an altered, smaller lattice constant for the MgPc ML, and considering the

gas-phase HOMO (which yields $t \approx 3$ meV), is effectively analogous to a spatial expansion of $\Psi_{\mathrm{HOMO}}(\mathbf{r})$ [resulting from MgPc-Ag(100) hybridization, consistent with previous work[3]]. This approach allows us to avoid challenges in estimating t via Eqn. 1 using DFT-calculated on-Ag(100) molecular orbitals, which have an intricate real-space morphology (in comparison with the gas-phase ones).[3] As mentioned above, the larger t retrieved from the fitting for the 2L could be explained by some degree of π-stacking between 1st and 2nd MgPc layers, enhancing interactions between MgPc's.

S4 Near-Fermi ARPES EDCs and TB Model for MgPc Monolayer (ML) and Bilayer (2L)

ARPES EDCs acquired for the 2L, for E_{B} near the Fermi level (Fig. S4a, b), can be fitted with a Fermi-Dirac distribution; we do not observe features related to the MgPc LUMOs (the single Gaussian fit parameters are unrealistically broad). That is, for the 2L top-layer, LUMOs are unpopulated and lie above the Fermi level, consistent with STS measurements (main text Fig. 2). For the ML (Fig. S4c, d), near-Fermi ARPES EDCs can be fitted by a sum of a Fermi-Dirac distribution and a Gaussian peak. We attribute the Gaussian peak to the MgPc LUMOs populated via Ag(100)-to-MgPc electron transfer,[3] consistent with STS measurements (main text Fig. 2).

In the following, we focus on the $k_{\parallel}$-dependent E_{B} position of the LUMO-related fit Gaussian peaks in Fig. S4c, d (Fig. S4e, f). Similar to the single-band TB model accounting for inter-HOMO hopping, we considered a nearest-neighbor TB model accounting for hopping between the populated LUMOs of the ML. The two-fold degeneracy of the LUMOs, $\Psi_{\mathrm{LUMO},1}(\mathbf{r})$ and $\Psi_{\mathrm{LUMO},2}(\mathbf{r})$, requires a two-band TB model taking into account four different hopping integrals between adjacent sites j and $j+1$ within the ML: $t_0 = \left\langle \Psi^{(j)}_{\mathrm{LUMO},1} | H_{\mathrm{int}} | \Psi^{(j)}_{\mathrm{LUMO},2} \right\rangle$; $t_1 = \left\langle \Psi^{(j\pm1)}_{\mathrm{LUMO},1} | H_{\mathrm{int}} | \Psi^{(j)}_{\mathrm{LUMO},1} \right\rangle$; $t_2 = \left\langle \Psi^{(j\pm1)}_{\mathrm{LUMO},2} | H_{\mathrm{int}} | \Psi^{(j)}_{\mathrm{LUMO},2} \right\rangle$; $t_3 = \left\langle \Psi^{(j\pm1)}_{\mathrm{LUMO},1} | H_{\mathrm{int}} | \Psi^{(j)}_{\mathrm{LUMO},2} \right\rangle$.

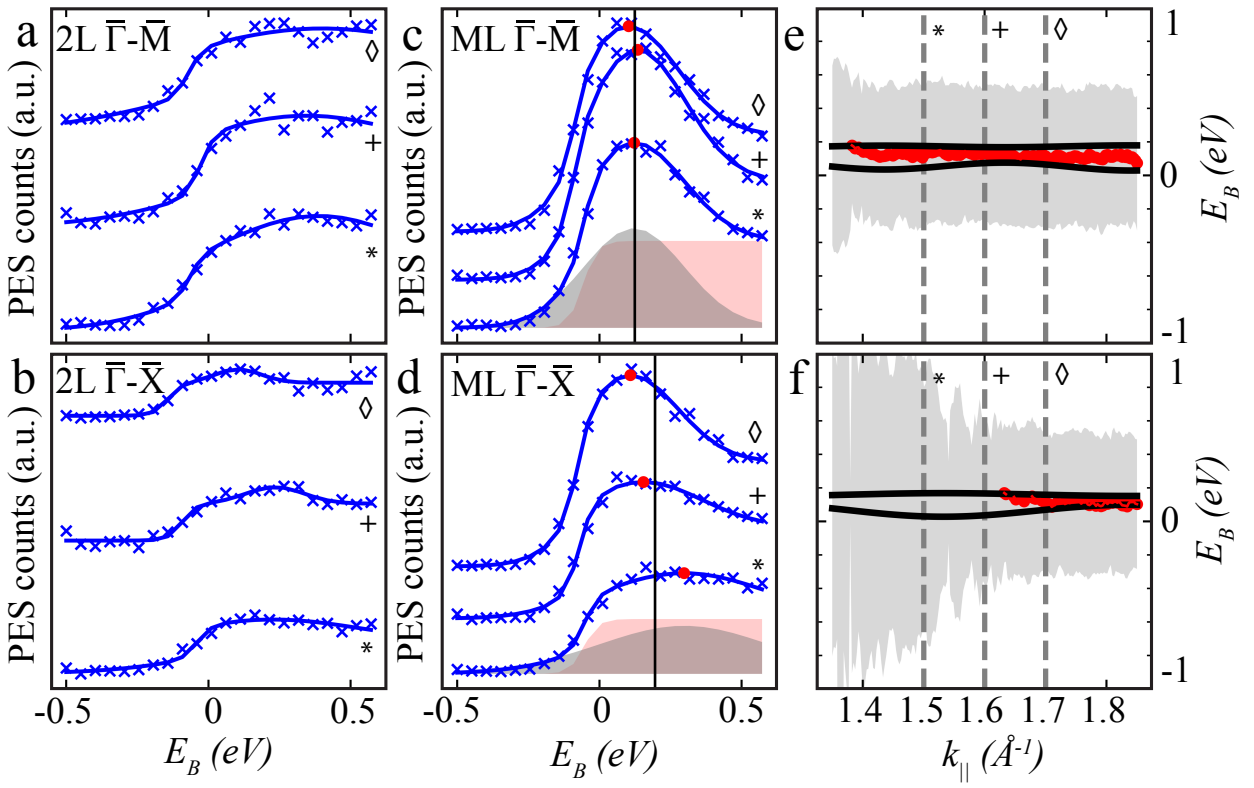

Figure S4: **Near-Fermi ARPES EDCs for MgPc monolayer (ML) and bilayer (2L): populated LUMOs features. a, b:** PES counts as a function of E_{B} for 2L, for E_{B} range near the Fermi level (upper white boxes in Fig. S3a, b) for different $k_{\|}$ along Ag(100) $\bar{\Gamma}-\bar{M}$ (a) and $\bar{\Gamma}-\bar{X}$ (b) orientations. Solid blue curve: fit to data composed of single Gaussian peak and Fermi-Dirac distribution (yielding unrealistically broad Gaussian peak). **c, d:** Same as (a, b), for ML (upper blue boxes in main text Fig. 4a, b). Curves offset for clarity. Blue crosses: experimental data. Solid blue curves: fit including Fermi-Dirac distribution (shaded red area) and single Gaussian peak (shaded grey area). Red dots: fit Gaussian peak energy positions. Black vertical line: average Gaussian peak energy position. Symbols match curves to $k_{\|}$ values indicated by grey vertical dashed lines in (e, f). **e, f:** Energy positions of near-Fermi fit Gaussian peak in (c, d) versus $k_{\|}$ along Ag(100) $\bar{\Gamma}-\bar{M}$ (e) and $\bar{\Gamma}-\bar{X}$ (f) orientations, for ML (red dots). Grey shaded region: full-width-at-half-maximum of Gaussian fits for different $k_{\|}$ in (c, d). Points for which fit standard error exceeded 12 meV were omitted. Solid black curves: energy dispersions resulting from two-band tight-binding model for hopping integrals calculated for LUMOs: resulting energy dispersion bandwidths are significantly smaller than experimental resolution.

The two TB energy dispersions $E_{1,2}(k_x, k_y)$ resulting from such inter-LUMO hopping are given by the eigenvalues of the following matrix:

$$\begin{bmatrix} E_0 + 2t_1 \cos(k_y \cdot b) + 2t_2 \cos(k_x \cdot b) & t_0 + 2t_3 (\cos(k_x \cdot b) + \cos(k_y \cdot b)) \\ t_0 + 2t_3 (\cos(k_y \cdot b) + \cos(k_x \cdot b)) & E_0 + 2t_1 \cos(k_x \cdot b) + 2t_2 \cos(k_y \cdot b) \end{bmatrix} \quad (2)$$

Here, E_0 is the eigenenergy of the LUMOs for a single isolated MgPc, and $t_0 = 47$, $t_1 = 3.5$, $t_2 = 5.1$ and $t_3 = -7$ meV were calculated by their definition above. In these calculations of $t_0, ..., t_3$, we considered DFT-calculated gas-phase $\Psi_{\mathrm{LUMO},1}(\mathbf{r})$ and $\Psi_{\mathrm{LUMO},2}(\mathbf{r})$,[3] and the same H_{int} as for the HOMO-related TB model, with a MgPc ML geometry (i.e., angle between MgPc isoindole-isoindole axis and MgPc ML unit cell vectors, Mg-Mg distance) slightly adjusted (with respect to that given by SPM and LEED measurements) such that $t = \left\langle \Psi^{(j\pm1)}_{\mathrm{HOMO}} | H_{\mathrm{int}} | \Psi^{(j)}_{\mathrm{HOMO}} \right\rangle$ calculated for the DFT-derived gas-phase HOMO matched the t from fitting the MgPc ML EDC data in Fig. 4 of main text (see above). The obtained LUMO-related, near-Fermi energy dispersions $E_1(k_x, k_y)$ and $E_2(k_x, k_y)$ are shown in Fig. S4e, f. Here, the two-fold degeneracy of the LUMOs, giving rise to these two TB-modeled near-Fermi bands (with bandwidths significantly narrower than the FWHM of the fit Gaussian peaks in Fig. S4c, d), hinders us to resolve (within our experimental conditions and energy resolution) the $k_{\|}$-dependent, LUMO-related energy dispersions $E_1(k_x, k_y)$ and $E_2(k_x, k_y)$, in contrast with the single HOMO-related band (main text Fig. 4, Fig. S3).

S5 LEED data of MgPc ML

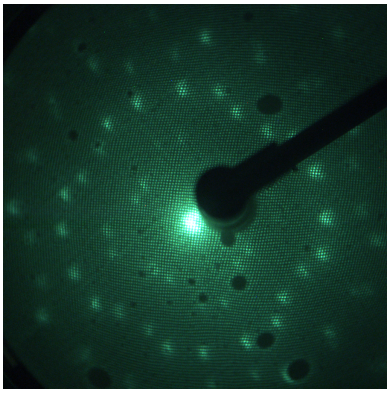

Figure S5: **LEED pattern of MgPc ML on Ag(100).** Same data as Fig. 1e of main text with no annotations or superimposed LEEDPat simulation features.

References

(1) Bussolotti, F.; Yang, J.; Yamaguchi, T.; Yonezawa, K.; Sato, K.; Matsunami, M.; Tanaka, K.; Nakayama, Y.; Ishii, H.; Ueno, N. et al. Hole-phonon coupling effect on the band dispersion of organic molecular semiconductors. *Nature Communications* **2017**, *8*, 173.

(2) Machida, S.-i.; Nakayama, Y.; Duhm, S.; Xin, Q.; Funakoshi, A.; Ogawa, N.; Kera, S.; Ueno, N.; Ishii, H. Highest-Occupied-Molecular-Orbital Band Dispersion of Rubrene Single Crystals as Observed by Angle-Resolved Ultraviolet Photoelectron Spectroscopy. *Physical Review Letters* **2010**, *104*, 156401.

(3) Castelli, M.; Hellerstedt, J.; Krull, C.; Gicev, S.; Hollenberg, L. C. L.; Usman, M.; Schiffrin, A. Long-Range Surface-Assisted Molecule-Molecule Hybridization. *Small* **2021**, *17*, 2005974.